Int J Adv Manuf Technol (2012) 60:473–485
DOI 10.1007/s00170-011-3633-7

ORIGINAL ARTICLE

Anisotropy of machined surfaces involved in the ultra-precision turning of single-crystal silicon—a simulation and experimental study

Minghai Wang · Wei Wang · Zesheng Lu

Received: 19 February 2011 / Accepted: 9 September 2011 / Published online: 18 October 2011

Abstract A new method was proposed for simulating the anisotropic surface quality of machined single-crystal silicon. This represents the first time that not only the mechanical properties of silicon, but also the crystal orientation, which is closely linked to the turning process, have been given consideration. In this paper, the crystallographic relationship between machined crystal planes and slip planes involved in ultra-precision turning was analyzed. The elasticity, plasticity, and brittleness properties of silicon in different crystal orientations were calculated. Based on the brittle–ductile transition mechanism of ultra-precision turning of single-crystal silicon, the orientation dependence of the surface quality of (111), (110), and (100) crystal planes were investigated via computer simulation. According to the simulation results, the surface quality of all machined planes showed an obvious crystallographic orientation dependence while the (111) crystal plane displayed better machinability than the other planes. The anisotropic surface properties of the (111) plane resulted from the continuous change of the cutting direction, which causes a change of actual angle between the slip/cleavage plane and machined plane. Anisotropic surface properties of planes (100) and (110) result from anisotropy of mechanical properties and the continuous changes of the cutting direction, causing the actual angle between slip/cleavage plane and machined plane to change simultaneously. A series of cutting experiments were carried out on the (111) and (100) crystal planes to verify the simulation results. The experimental results showed that cutting force fluctuation features and surface roughness are consistent with the anisotropy characteristics of the machined surface as revealed in simulation studies.

Keywords Anisotropy · Surface quality · Ultra-precision turning · Single-crystal silicon · Simulation and experimental

M. Wang (✉) · W. Wang
College of Mechanical and Electrical Engineering,
Shenyang Aerospace University,
110136 Shenyang, People's Republic of China
e-mail: wmh@sau.edu.cn

M. Wang · Z. Lu
College of Mechanical and Electrical Engineering,
Harbin Institute of Technology,
15001 Harbin, People's Republic of China

1 Introduction

During the practical application of optical components, anisotropy of optical crystal materials has become a problem in urgent need of attention. A number of studies have achieved ductile mode cutting of silicon using micro-turning processes [1–13]. However, in the research field of ultra-precision machining, few studies have analyzed the anisotropy of surface quality relative to the mechanism of brittle–ductile transition. The research team led by Scattergood earlier discovered and explained surface anisotropy [14–16]. Blackley and Scattergood explained the orientation-dependent machining damage in silicon by examining the variation in resolved tensile stress on the {1 1 1} slip planes [16]. In recent years, academics have begun to pay attention to this phenomenon, and through qualitative analysis of the relative change between the cutting direction and the crystal structure of single-crystal materials, to explain the reasons behind anisotropy of silicon crystal surface roughness [17, 18]. Shibata et al. carried out diamond turning of single-crystal silicon along all the crystallographic directions on the (001) and (111)

planes. The experimental results showed that the orientation dependence of the machined surface takes the form of a fourfold symmetric and threefold symmetric cross through the center on the (001) and (111) wafer surface, respectively. They qualitatively explained the direction-dependent damage effects by the use of a slip model [17]. To investigate the nature of the chip formation process with crystal orientation, molecular dynamics simulations of nanometric cutting on single-crystal aluminum were conducted by Komandurib et al. The results showed that extensive dislocation occurred ahead of the cutting tool, principally along, normal to, along and normal to, or at −45°or −60° to the cutting direction, depending on the specific orientation and direction of cutting [19]. Hung and Fu studied the effect of crystallographic orientation in ductile regime machining of (100) silicon wafer. They found that ductile regime machining could be achieved when cutting along the <110> directions and pits were observed when cutting along the <100> directions [20]. Cheung also carried out face cutting experiments on silicon single crystals with different crystallographic orientations. Experimental results indicated that the anisotropy of surface roughness occurs when the cutting direction relative to the crystallographic orientation varies successively in diamond turning [21]. O'Connor et al. measured the critical chip thickness as a function of crystallographic orientation on the (0 0 1) cubic face. Experimental results showed that the critical chip thickness in silicon for ductile material removal reaches a maximum of 120 nm in the [1 0 0] direction and a minimum of 40 nm in the [1 1 0] direction [22]. After carrying out sets of cutting trials, Marsh et al. concluded that the underlying four-lobe symmetry of the (1 0 0) crystal plane is clearly visible in the force and AE signatures, and that this results from the anisotropic variation in material properties of the Si crystal [23]. However, the binding force between silicon atoms comprises covalent bonds, so the distances between atomic surfaces in different crystal planes are different, and the distance between atoms in different crystallographic directions is also different, resulting in the physical and mechanical properties of silicon in different crystallographic directions being anisotropic.

The orientation dependence of machined surfaces, apart from being related to the change of cutting force imposed on the slip plane and slip direction resulting from the relative change between the cutting direction and the crystal structure of single crystal materials, is also related to the anisotropy of physical and mechanical properties. Research into the brittle–ductile transition mechanism suggests that single-crystal silicon under action of a diamond tool will emit a number of dislocations before silicon fracture [24, 25]. Consequently, by studying the contrast of the number of dislocations emitted from different crystal planes or different crystallographic directions, the orientation dependence of plastic deformation capacity or machined surface quality involved in ultra-precision machining single-crystal silicon can be demonstrated in a more accurate description.

In this paper, based on the previous studies of the brittle–ductile transition mechanism, a simulation approach is proposed for clarifying the nature of anisotropy of machined surfaces involved in the ultra-precision turning of single-crystal silicon. Firstly, the crystallographic orientation relationships between the machined crystal plane and slip planes were analyzed when cutting along different crystal planes and the actual angles θ' between machined plane and the {111} planes were calculated. The elasticity, plasticity, and brittleness properties of silicon involved in machining were calculated. Secondly, based on fundamental theories and methods for studying the brittle–ductile transition mechanism investigated in previous studies, a simulation of plastic deformation and brittle fracture behavior along different machined crystal planes and crystallographic directions involved in the ultra-precision turning process was performed, and the anisotropies of surface properties derived by analyzing the distribution of the emitted dislocations. Finally, verification experiments were performed, with the experimental results showing good agreement with the simulation results.

1.1 Crystallographic orientation relationships

To reveal the orientation dependence of ultra-precision machined surfaces, the crystallographic orientation relationships between the machined crystal plane and slip planes need to be analyzed when cutting along different crystal planes. Single-crystal silicon has an octahedral crystal structure, where the {111} planes comprise the slip planes and cleavage planes. The angle between the {111} planes and {100} planes is equal to 54.74° while the angle between the {110} planes and {111} planes is equal to 35.26°; the angle between different {111} planes is equal to 70.52°.

The relationships between the machined crystal planes and slip planes are shown in Fig. 1, when cutting along (100), (110), and (111) crystal planes, respectively.

According to the brittle–ductile transition mechanism involved in the ultra-precision turning of silicon, the deformation behavior of silicon under cutting force is an interaction between crack propagation and dislocation movement [24, 25]. Under the plane-strain condition, assuming a composite load, depending on the cutting path direction and based on the analysis of silicon crystal structure, a model of the stress intensity factor k_{I} and k_{II} at the top of the crack contained in silicon is established as shown in Fig. 2.

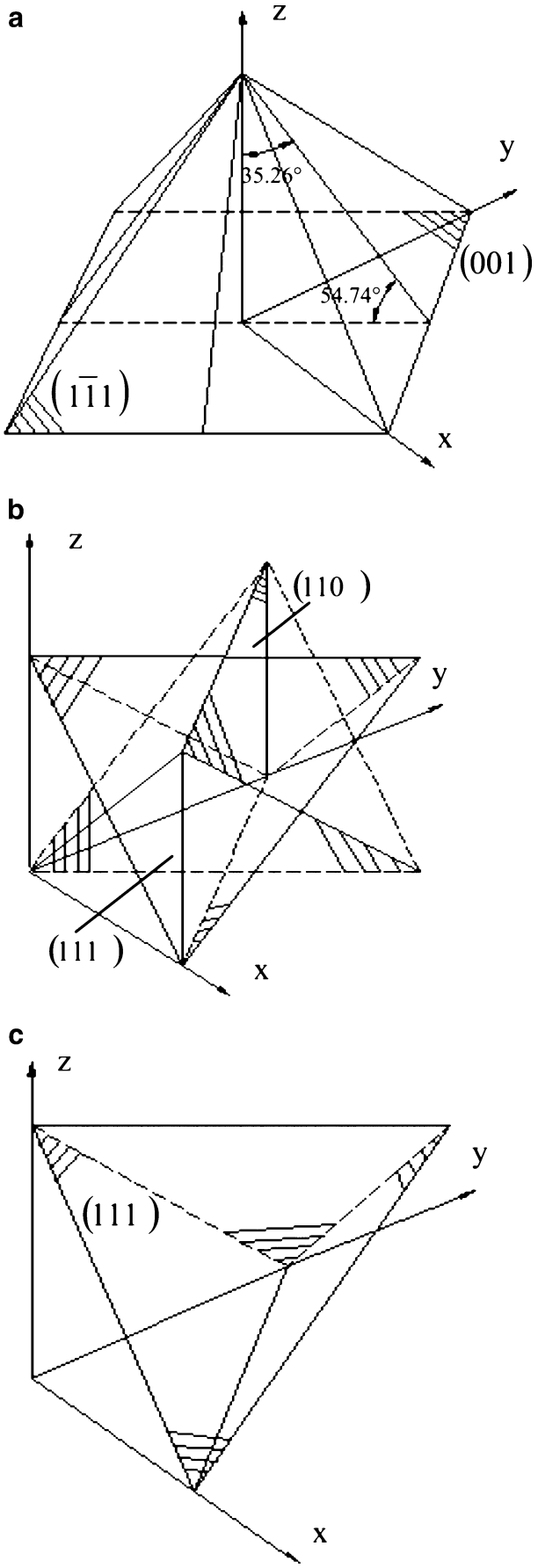

Fig. 1 Relationships between the machined crystal planes and slip planes: **a** between (100) and {111} planes; **b** between (110) and {111} planes; **c** between {111} crystal planes

Under the plane-strain condition, when cutting direction changes by angle $\Delta\theta$ along the machined plane, the actual angle θ' between the machined plane and the {111} planes as shown in Fig. 2 can be calculated as follows:

$$\left(\frac{\sin\theta'}{\sin\theta}\right)^2 + \cos^2\theta'\sin^2\Delta\theta = 1 \tag{1}$$

Where θ' is the angle between the machined plane and (111) slip plane after cutting direction change $\Delta\theta$, and θ is the initial angle between the machined plane and {111} slip planes.

It is obvious that the angle between the machined plane and (111) slip crystal plane will be different when different crystal planes are chosen as the machined plane. At the same time, under plane-strain conditions, the actual angle will vary continuously with the continuous changes in cutting direction. From the above analyses, the cutting component force on the machined plane and crystal slip plane changes with the change of cutting direction; in other words, under the action of the cutting force the behavior of slip deformation and cleavage fracture also changes with change of cutting direction.

1.2 Anisotropic mechanical properties of single-crystal silicon

Binding forces between silicon atoms comprise strict directional covalent bonds, which result in the mechanical properties of silicon in different cutting directions exhibiting differences [26]. The mechanical properties of silicon as relevant to machining are chiefly elasticity, plasticity, and

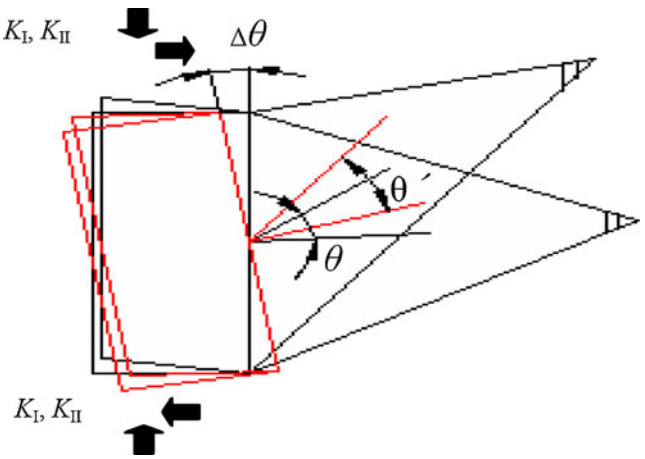

Fig. 2 The relational model of crack plane and slip planes—cutting path direction factor

brittleness. The fracture toughness of silicon is obtained by the following formula [27]:

$$K^2{}_{\text{cleave}} \approx 4G\frac{Ea_0}{72(1-2\nu)} \tag{2}$$

Where a_0 is constant and equal to 0.543 nm, ν is Poisson's ratio, E is Yang's elastic modulus, and G is the shear modulus. The critical stress intensity factor needed for crack emitting dislocation is shown as follows [28]:

$$K_{\text{IIe}} = \left(\frac{2Gr_{\mu s}}{1-\nu}\right)^{1/2} \tag{3}$$

Where $\gamma_{\mu s}$ is the unstable stacking energy of the slip plane,$\gamma_{\mu s} = \frac{Gb^2}{2\pi^2 h}$, and b is the Burgers vector. The Burgers vector of three crystal planes respectively can be calculated by $b_{111} = 1/2a_0$, $b_{110} = \sqrt{2}/2a_0$, and $b_{100} = a_0$, respectively.

The elastic modulus and Poisson's ratio can be calculated as follows:

$$\frac{1}{E} = S_{11} - 2\left[(S_{11}-S_{12}) - \frac{1}{2}S_{44}\right]\left(l_1{}^2l_2{}^2 + l_2{}^2l_3{}^2 + l_3{}^2l_1{}^2\right) \tag{4}$$

$$\nu = -E\left[S_{12} + \left(S_{11} - S_{12} - \frac{1}{2}S_{44}\right)\left(l_1{}^2m_1{}^2 + l_2{}^2m_2{}^2 + l_2{}^2m_2{}^2\right)\right] \tag{5}$$

where S_{ij} is the flexibility factor, and $S_{11}=0.768\times 10^{-11}$ Pa^{-1}, $S_{12}=-0.214\times 10^{-11}$ Pa^{-1}, $S_{44}=1.256\times 10^{-11}$ Pa^{-1}, l_i is crystallographic direction cosine, and i= 1,2,3; m_i is the direction cosine of crystal direction orthogonal to crystallographic direction, and i=1,2,3.

The elastic modulus and shear modulus of three crystal planes with varying crystal orientation are shown in Fig. 3. Figure 3 indicates that the elastic modulus and shear

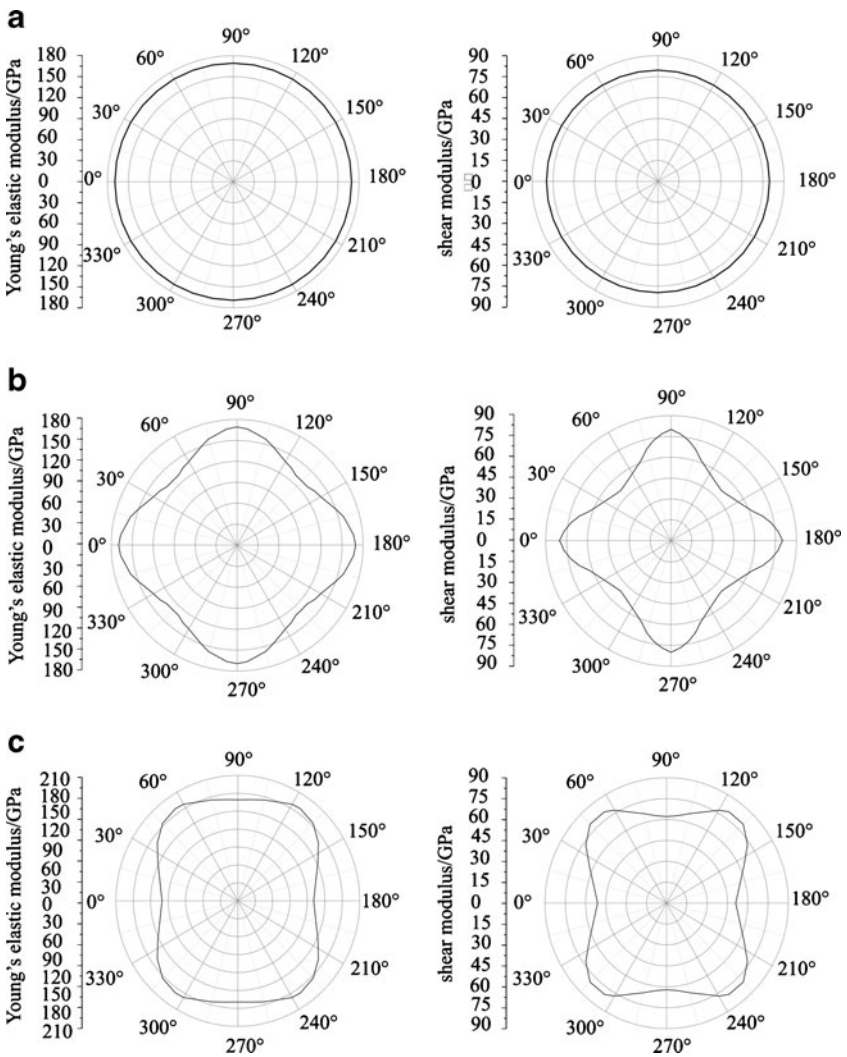

Fig. 3 Young's modulus and shear modulus: **a** (111) plane, **b** (100) plane, and **c** (110) plane

modulus of (111) plane are the same in all crystallographic directions, while the elastic modulus and shear modulus of the (100) and (110) planes in different crystallographic directions are quite different. It is not difficult to obtain brittleness and plasticity properties of different crystal planes and in different crystallographic directions by substituting the elastic modulus and shear modulus into Eqs. 2 and 3.

1.3 Simulation study methods

The basic theories and methods for studying the brittle–ductile transition mechanism given in the references [24, 25] (i.e., given by Eqs. 6–14) were also used for the simulation study of anisotropic surface quality during the ultra-precision turning of single-crystal silicon. However, the important idea is that depending on the different crystal plane selected as the machined surface, when the cutting direction changes continuously, according to Eq. 1, the actual angle θ' between machined plane and the slip cleavage planes can be calculated, and the various mechanical properties along the cutting direction can then also be obtained from Eqs. 2–5. Following, the results are substituted into Eqs. 6–14, thus completing the simulation of plastic deformation and brittle fracture behavior along different machined crystal planes and crystallographic directions involved in the ultra-precision turning process.

In the process of precision cutting silicon, the crystal material is subject to the pressure-shear loading condition as shown in Fig. 2. The stress on the slip plane under the conditions of additional load k_{I}, k_{II} can be calculated using Eqs. 6 and 7 [29].

$$\sigma_\theta = \frac{1}{2\sqrt{2\pi r}} \cos\frac{\theta'}{2}\left[k_{\mathrm{I}}(1+\cos\theta') - 3k_{\mathrm{II}}\sin\theta'\right] \tag{6}$$

$$\sigma_{\mathrm{r}\theta} == \frac{1}{2\sqrt{2\pi r}} \cos\frac{\theta'}{2}\left[k_I \sin\theta' + k_{II}(3\cos\theta' - 1)\right] \tag{7}$$

Where σ_θ is normal stress, $\sigma_{\mathrm{r}\theta}$ is shear stress, and r is the distance to the crack tip. If the dislocation is emitted from the crack tip, the stress intensity factors contributed by an emitted dislocation along slip plane are [30]

$$k_{Is} = \frac{1}{2\sqrt{2\pi r_c}} \frac{\mu b_e}{(1-\nu)} 3\sin\theta\cos\frac{\theta'}{2} \tag{8}$$

$$k_{IIs} = -\frac{1}{2\sqrt{2\pi r_c}} \frac{\mu b_e}{(1-\nu)} (3\cos\theta' - 1)\cos^2\frac{\theta'}{2} \tag{9}$$

where b_{e} is the Burgers vector of an edge dislocation alone the slip direction and r_{c} is the distance from the crack tip to the edge dislocation. Wang defines the stress intensity factors K_{I} and K_{II} as follows: [31]

$$K_{I(Is)} = \lim_{r\to 0}\left[\sqrt{2\pi r}\sigma_\theta\right] \tag{10}$$

$$K_{II(IIS)} = \lim_{r\to 0}\left[\sqrt{2\pi r}\sigma_{r\theta}\right] \tag{11}$$

Using Eqs. 6–11, K_{I} and K_{II} and K_{Is} and K_{IIs} can be obtained. K_{Is} and K_{IIs} are the stress intensity factors due to the emitted dislocations, and $\mathrm{K_I}$ and $\mathrm{K_{II}}$ are the stress intensity factors applied on the tip of the crack by external loading.

Rice and Thomson [28] suggested that the applied stress intensity factor should be large enough so that dislocation can be emitted through the region near the crack tip. In other words, a critical stress intensity factor needed for dislocation emission is

$$K^{\mathrm{tip}}{}_{II} = K_{IIe} \tag{12}$$

where K_{IIe} is given by Eq. 3.

The emitted dislocation modifies the stress of the crack tip such that the stress intensity factors are shielded from the applied stress as follows: [32]

$$K^{\mathrm{tip}}{}_I = K_I + K_{Is} \tag{13}$$

$$K^{\mathrm{tip}}{}_{II} = K_{II} + K_{IIs} \tag{14}$$

The Sih's fracture criterion is taken [33] as the fracture criterion.

In general, atomically sharp cracks are formed by the breaking of covalent bonds when a load acts upon Si single crystals. A Si single crystal will plastically deform as long as dislocation can be emitted from the atomically sharp cracks, otherwise the cracks will propagate. As externally applied stress intensity increases, the processes of dislocation emission and the crack cleavage involved at the crack tip can be described as follows, according to the results of the simulation. The crack tip emits dislocations which can shield it from external loading and protect it from propagation, so that two processes coexist at the crack tip: the increase in the crack tip stress intensity; and the shielding of the crack tip field due to dislocation emission. Firstly, the crack tip stress intensity increases with the applied stress intensity until the critical stress intensity for dislocation emission given by Eq. 12 is reached. The dislocation emitted from the crack tip shields the crack tip field, the local stress intensity factors as given by Eqs. 13 and 14 decrease, and the ductile mode prevails. When the applied stress intensity increases further, the crack tip stress

intensity increases again, and the dislocations are emitted one after the other, resulting in a cyclic process. If the shielding due to dislocation motion is not sufficient to offset the increase in the crack tip stress intensity, then the fracture criterion as given by Sih's fracture criterion is met and brittle fracture occurs.

The flow chart of simulation is depicted in Fig. 4.

2 Results of simulation and discussion

2.1 (111) plane

The [112] crystallographic direction was chosen as the initial cutting direction when simulating anisotropy of surface properties during machining of the (111) plane, and −40° and −25° negative rake angle cutting tools were adopted in the simulation, with the results shown in Fig. 5. Assume that the cutting tool on the (111) crystal plane turns 360° continuously counter-clockwise, and the initial position named as 0° position in simulation study can be set to the [112]crystallographic direction. Thus, when the cutting tool rotates 30°, 60°, 90°, and 120°, the cutting directions are the [101], [211], [110], and [121] crystallographic directions, respectively.

Simulation results showed that the distribution of the total number of emitted dislocations and the number of dislocations emitted from the machined crystal plane and slip plane simultaneously formed six peaks regardless of whether loaded with the −40° or −25°negative rake angle cutting tool.

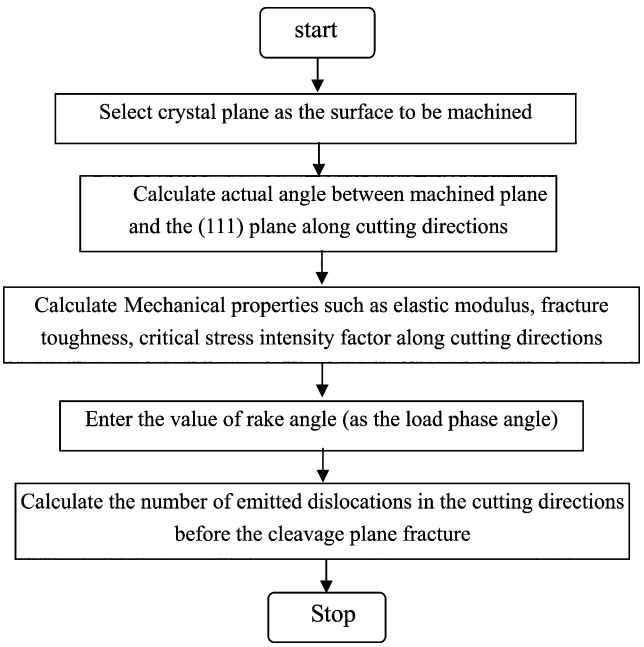

Fig. 4 Flow chart of simulation of anisotropic surface quality

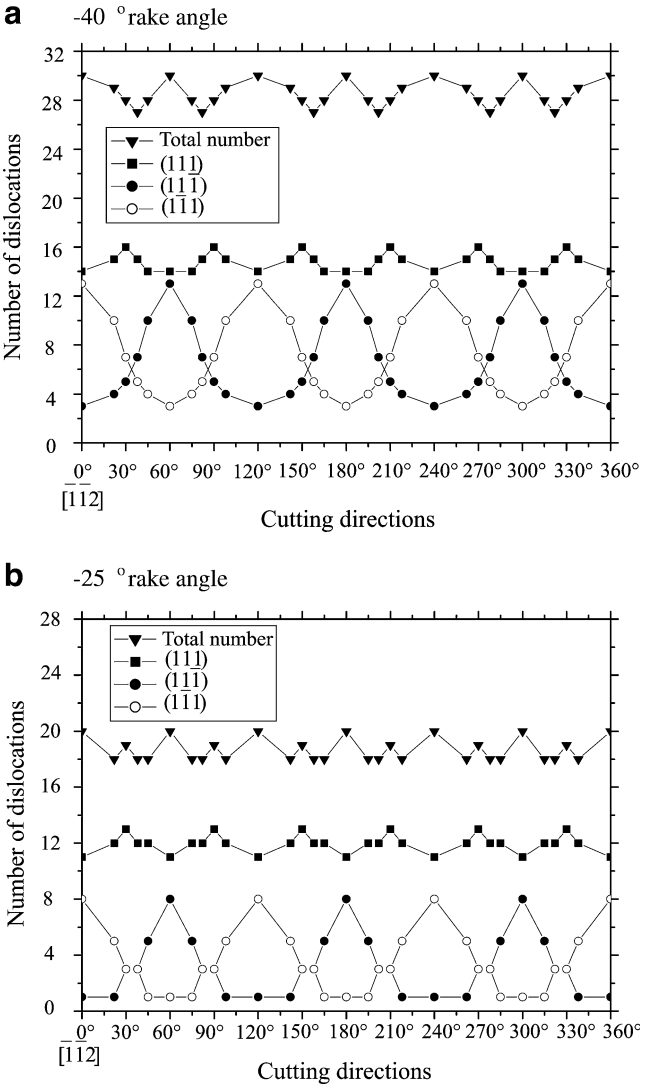

Fig. 5 Relationship between numbers of dislocations and cutting directions during the turning of the (111) crystal plane in **a** −40° and **b** −25° rake angle

The mechanism of orientation dependence of machined surface quality can be illustrated by observing the distribution of the number of emitted dislocations. The distribution of dislocations in the range of 0–60° is taken as an example. From both sides of the [112] crystallographic direction to within 15°, only a small number of dislocations are emitted from the machined plane, and moreover, the number of dislocations emitted from the machined plane and slip plane is very uneven. As a comparison, from both sides of [101] crystallographic direction to within 15°, a greater number of dislocations is emitted from the machined plane, and moreover, the number of dislocations emitted from the machined plane is relatively consistent with the slip planes.

The above analyses indicate that inadequate and uneven plastic deformation occurs in the [112] crystallographic

direction, and it can be inferred that surface roughness is relatively large when cutting along directions having the same mechanical properties and crystallographic relationship.

Contrastively, more adequate and uniform plastic deformation occurs in the [101] crystallographic direction, and it can be inferred that surface roughness is relatively small when cutting along directions having the same mechanical properties and crystallographic relationship.

In fact, the elastic modulus and shear modulus are completely the same in all crystallographic directions in the (111) crystal plane, and the critical stress intensity factor of dislocation emission and fracture toughness are also the same. Therefore, the anisotropic surface properties of the machined (111) plane is due to the continuous change in the cutting direction leading to the actual angle between slip/cleavage plane and machined plane changing simultaneously, which accordingly results in a different extent of plastic deformation and cleavage fracture cleavage occurring on the machined plane and slip/cleavage plane.

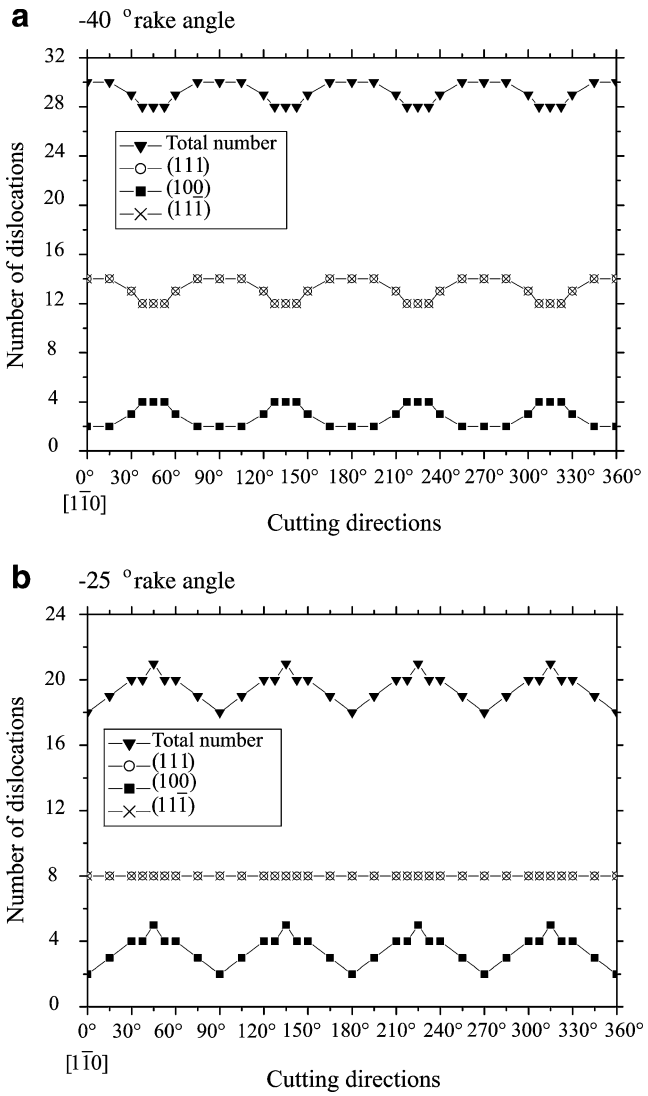

Fig. 6 Relationship between numbers of dislocations and cutting directions during the turning of the (100) crystal plane in **a** −40° and **b** −25°rake angle

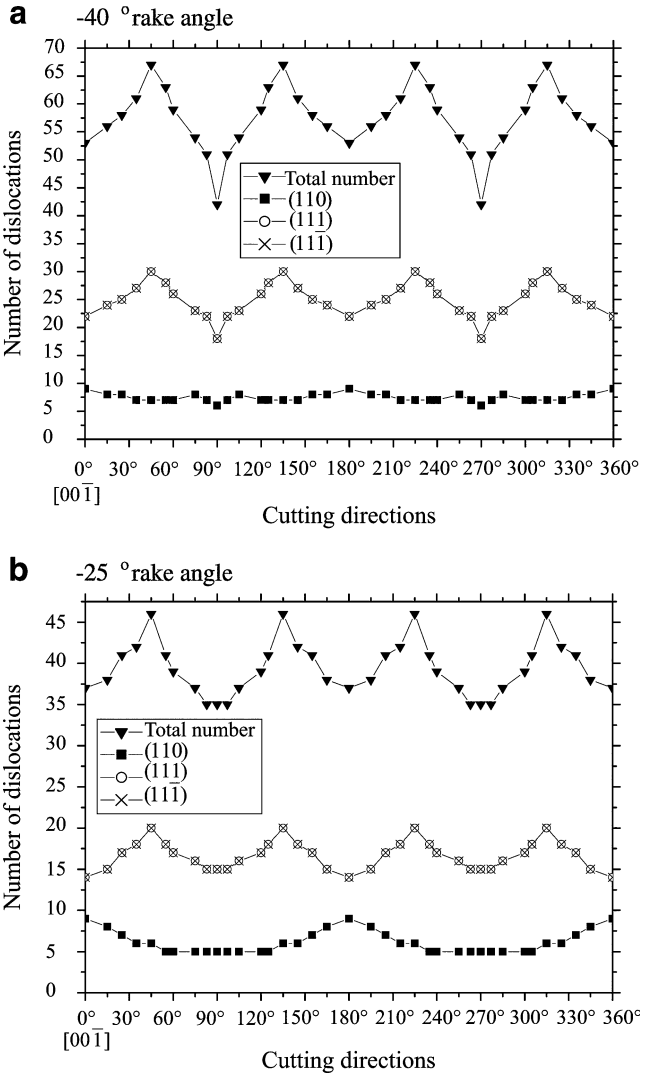

Fig. 7 Relationship between numbers of dislocations and cutting directions during the turning of the (110) crystal plane in **a** 40° and **b** −25°rake angle

2.2 (100) plane

The [110]crystallographic direction is defined as the initial position in the simulation study on the machining (100) plane and turning of the (100) crystal plane 360° continuously counter-clockwise. Thus, when the cutting tool rotates 45° and 90°, the cutting directions are the [010] and [110] crystallographic directions respectively; results are shown in Fig. 6.

Simulation results showed that graphs of the dislocations distribution exhibit two-axis symmetry. The distribution of

dislocations in the range of 0~90° are taken as an example. From both sides of the [110] crystallographic direction to within 15°, a small number of dislocations are emitted from the machined plane, and moreover the number of dislocations emitted from the machined plane and slip planes is very uneven. As a comparison, from both sides of the [010] crystallographic direction to within 15°, a relatively larger number of dislocations are emitted from the machined plane, and moreover, the number of dislocations emitted from the machined plane is relatively consistent with those from the slip planes.

The above analyses indicate that inadequate and uneven plastic deformation occurs along the [110] crystallographic direction; similarly, surface roughness is relatively large when cutting along directions having the same mechanical properties and crystallographic relationship. Contrastively, more adequate and uniform plastic deformation occurs along the [010] crystallographic direction, and similarly, surface roughness is relatively small when cutting along directions having the same mechanical properties and crystallographic relationship.

Furthermore, the number of dislocations emitted from the (100) plane is less than from (111), which indicates that the (111) plane is more easily machined than the (110) plane.

Unlike the case with the (111) crystal plane, the elastic modulus and shear modulus are anisotropic in the (100) crystal plane, and the critical stress intensity factor of dislocation emission and the fracture toughness are also anisotropic. Therefore, the anisotropic surface of the machined (100) plane is due to anisotropy of mechanical properties and the continuous changes of the cutting direction causing the actual angle between slip/cleavage plane and machined plane to change simultaneously, which accordingly results in a different extent of plastic deformation and cleavage fracture cleavage occurring on the machined plane and slip/cleavage plane.

The simulation results of machining (111) and (100) plane also show that the crystallographic relationship and mechanical properties of the machined plane and slip/cleavage plane jointly play a significant role in the orientation dependence of machined surface quality.

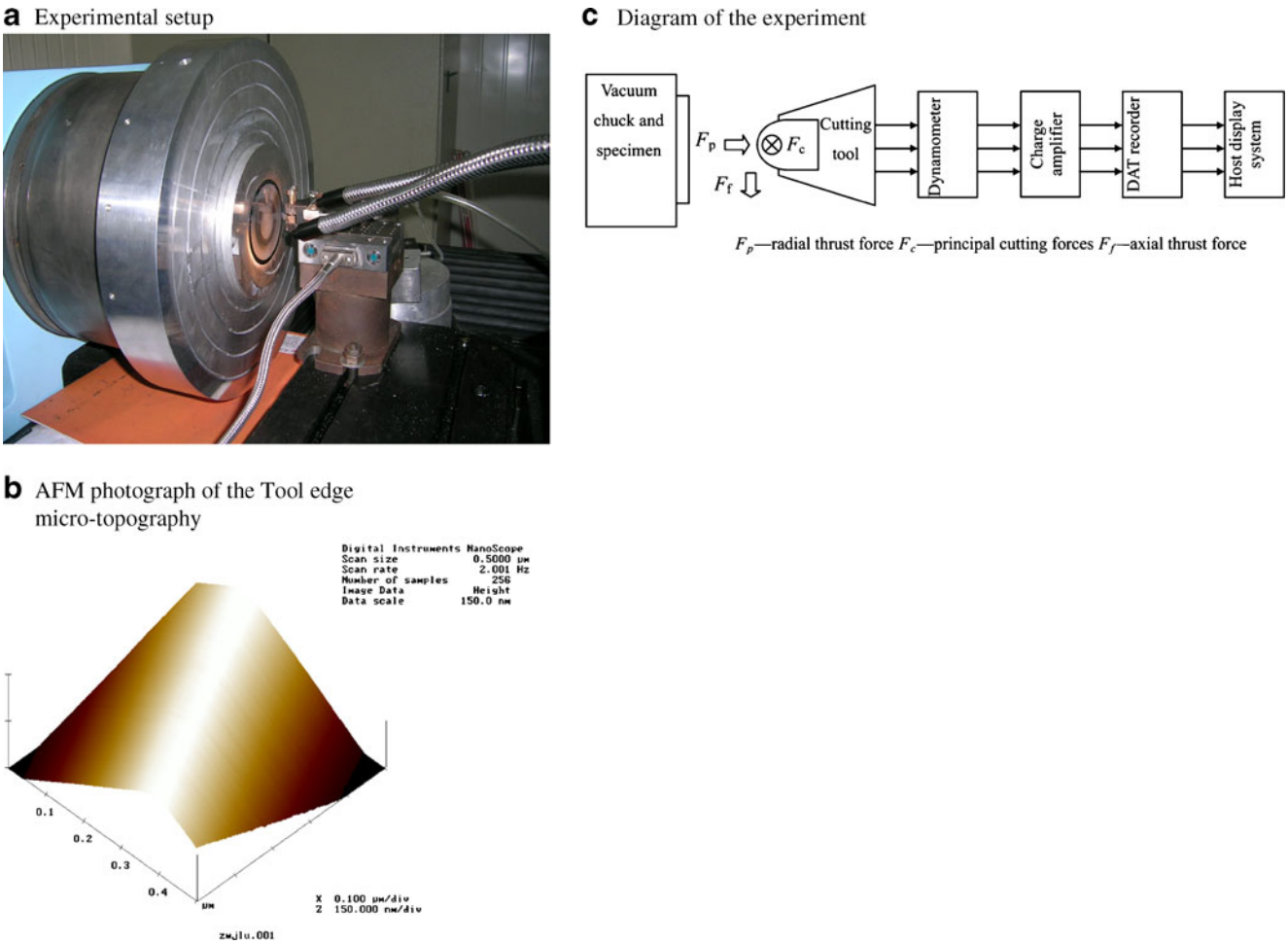

Fig. 8 Experimental setup schematic. **a** Experimental setup. **b** AFM photograph of the tool edge micro-topography. **c** Diagram of the experiment

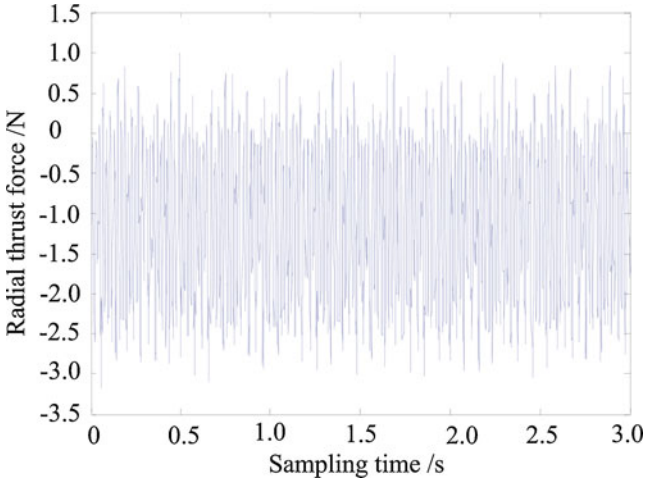

Fig. 9 Measured radial thrust force

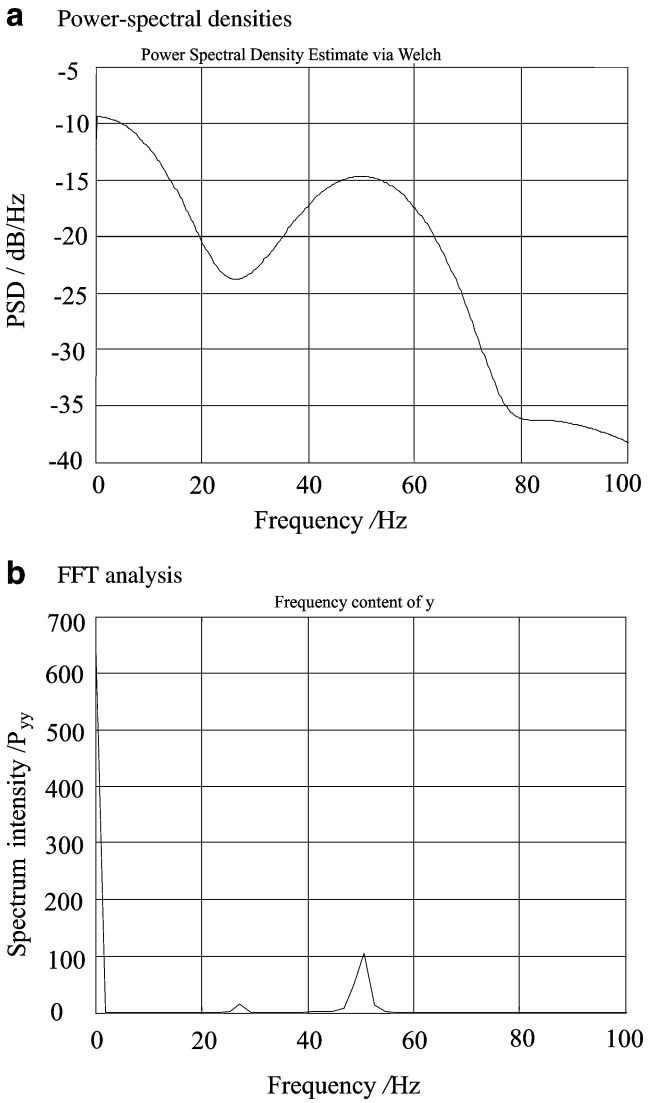

Fig. 10 PSD and FFT analysis of signal of cutting force. **a** Power-spectral densities. **b** FFT analysis

2.3 (110) plane

The [001]crystallographic direction is defined as the initial position in the simulation study on the machining (110) plane and turning of the (110) crystal plane 360° continuously counter-clockwise. Thus, when the cutting tool rotates 55° and 90°, the cutting directions are the [111] and [110] crystallographic directions, respectively; results are shown in Fig. 7.

Similar to simulation (100), the results showed that graphs of the dislocations distribution have two-axis symmetry. The distribution of dislocations in the range of 0–90° is taken as an example.

From both sides of the [110] crystallographic direction to within 15°, a small number of dislocations are emitted from the machined plane. As a comparison, from both sides of [111] crystallographic direction to within 30°, a larger number of dislocations are emitted from the machined plane, however the number of dislocations emitted from the machined plane is significantly less than from the slip planes.

The above analyses indicate that inadequate and uneven plastic deformation occurs along the [110] crystallographic direction; similarly, surface roughness is relatively large when cutting along directions having the same mechanical properties and crystallographic relationship.

Contrastively, more adequate and uniform plastic deformation occurs along the [111] crystallographic direction, and similarly, surface roughness is relatively small when cutting along the directions having the same mechanical properties and crystallographic relationship.

The simulation results of machining the (110) surface showed the total number of dislocations to be greater in comparison with machining the (111) plane. However, a cleavage fracture occurs along the (111) crystal plane and perpendicular to the (110) plane, hardly emitting any dislocations. This phenomenon was discovered in the process of simulation when the fracture criteria adopted in simulation program [23] were met. Moreover, the number of dislocations emitted from the machined (110) plane is significantly less than that from the machined (111) plane,

Table 1 Cutting conditions

Specimen	(111) and (100)crystal plane of silicon substrate	
Diamond tool	Rake angle of −40°; cutting edge radius is 50 nm; tool nose radius is 2.6 mm	
Cutting conditions	Spindle rotation speed, 600 rpm	
	(111) plane	Cutting depth, a_p=5 μm; feed speed, f=2 μm/rev
	(100) plane	Cutting depth, a_p=3 μm; feed speed, f=0.8 μm/rev

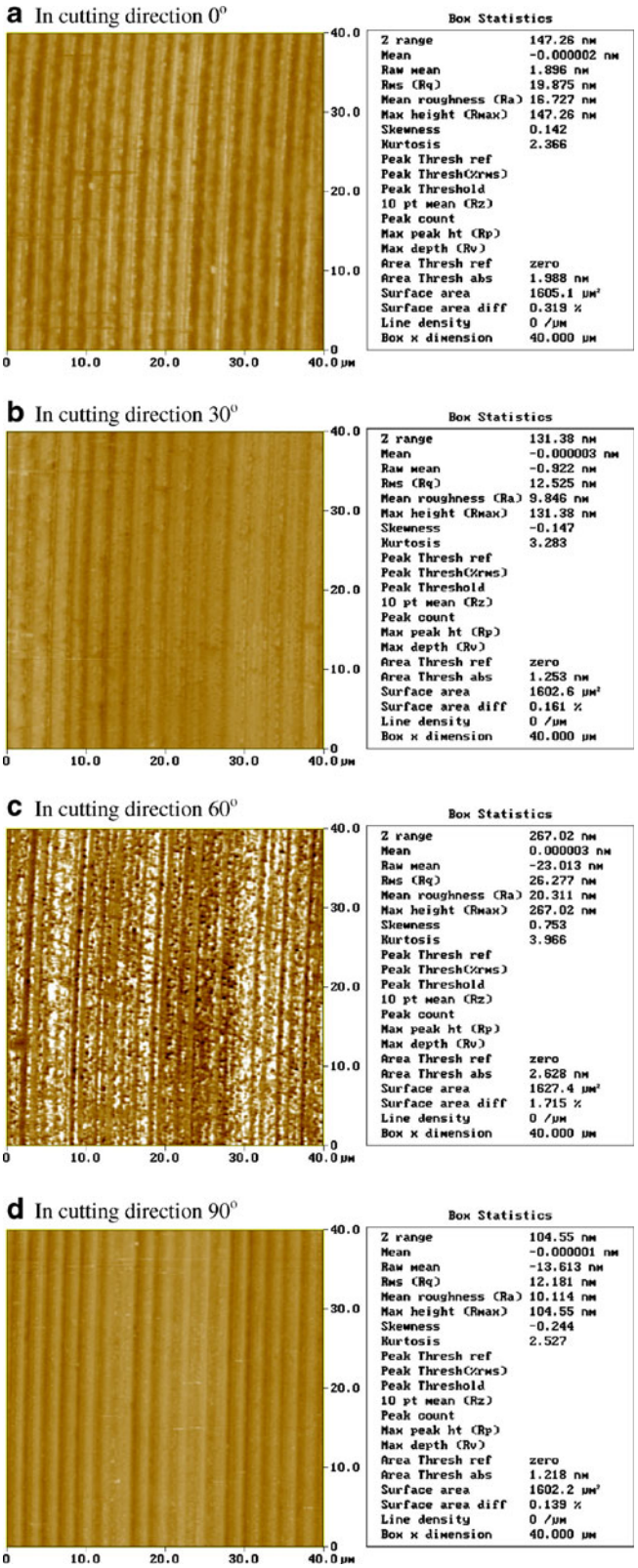

Fig. 11 AFM images of the machined (111) plane in a cutting direction of: **a** 0°, **b** 30°, **c** 60°, and **d** 90°

and the distribution of the dislocations between the machined crystal plane and the slip planes during turning of the (110) plane is always less uniform than that derived from turning of the (111) plane. Therefore, cutting surface quality is also poor when machining along the (110) plane.

3 Experimental study

3.1 Cutting force experiment

The simulation results have shown that the anisotropy of surface quality results from the variation in machinability of different cutting directions. The extent of the plastic deformation of silicon can be clearly reflected in the fluctuation of cutting force. Therefore, if the fluctuation feature of cutting force can be determined by experiments, it can provide a basis for further research.

The cutting force experiments were conducted by face turning the specimen on a numerically controlled ultra-precision lathe (Harbin Institute of Technology, China). A diagram illustrating the experimental setup is shown in Fig. 8. Experiments were performed on the (111) wafer, which is mounted on a vacuum chuck. The diamond tools used in the face turning experiments had rake angle of −40° and a clearance angle of 5°. The radius of the unused cutting edge was 50 nm. The cutting forces were measured using a KISTLER Mini-3-D dynamometer (Type-9256A) in conjunction with a KISTLER three-channel charge amplifier and a DAT recorder. Figure 9 is a graph showing the measured values of radial thrust force during the ultra-precision machining of silicon under the given cutting conditions; spindle speed, n=500 rpm; depth of cut, a_p= 5 μm; and feed rate, f=2 μm/rev.

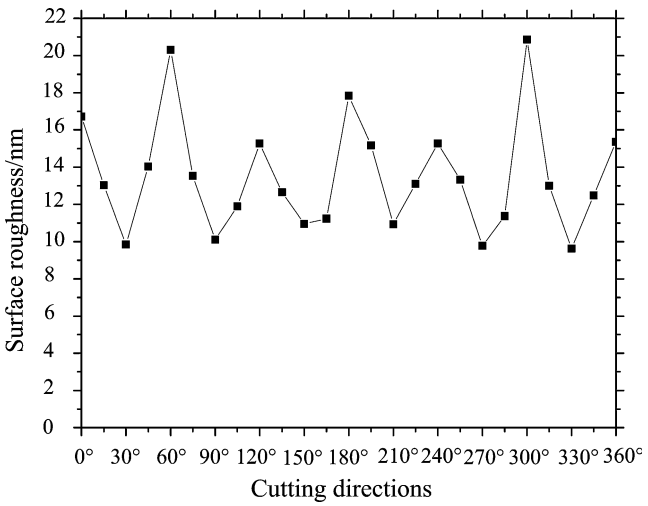

Fig. 12 Relationship between the surface roughness and cutting direction on the (111) plane

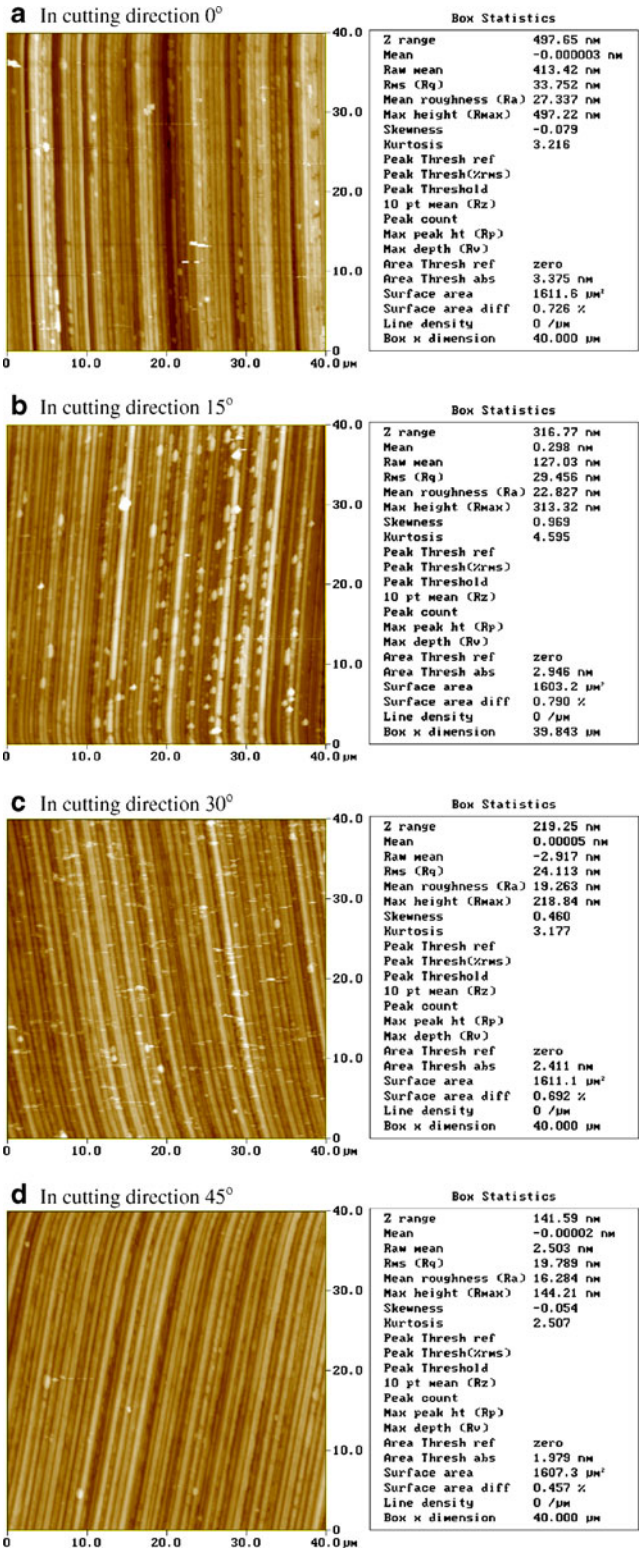

Fig. 13 AFM images of the machined (100) plane in a cutting direction of **a** 0°, **b** 15°, **c** 30°, and **d** 45°

The results of power-spectral density (PSD) and discrete FFT analysis of the force signal are shown in Fig. 10.

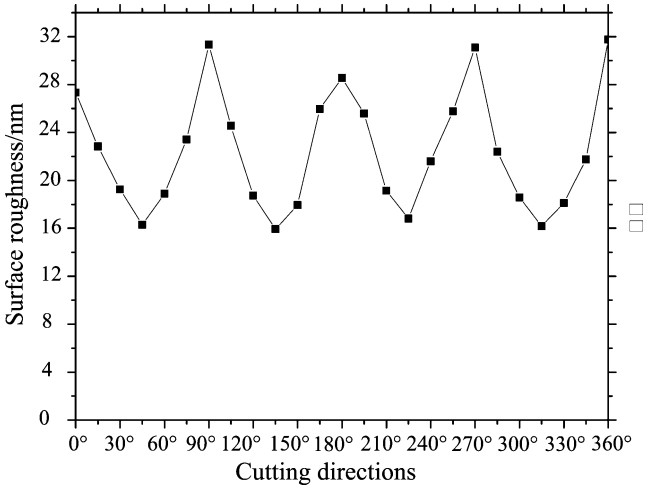

Fig. 14 Relationship between the surface roughness and cutting direction on the (100) plane

As can be seen from Fig. 10, with the exception of 0 Hz (resulting from low-frequency interference signals), the maximum PSD and a large harmonic component appear around the 50 Hz frequency.

The frequency f_s of spindle rotation:

$$f_s = v_c/60 = 50/6 \text{ Hz} \tag{15}$$

The frequency of cutting force fluctuation f_f is equal to 50 Hz. The fluctuation frequency of greater cutting force is thus six times that of spindle rotation, indicating that the surface quality of the machined (111) plane will take the shape of six parts significantly different in comparison with other the parts.

3.2 Experimental research on anisotropy of surface properties

In order to verify the simulation results for anisotropy of surface properties in the ultra-precision machining of single-crystal silicon, face turning experiments were performed on silicon (111) and (100) crystal plane, with turning conditions shown in Table1.

The surface roughness of the machined specimen was measured by atomic force microscopy, with scan range of 40×40 μm. Under the cutting conditions mentioned previously in Table 1, the AFM images of the surface topography of the (111) plane in cutting directions 0°, 30°, 60°, and 90° are displayed in Fig. 11. A schematic diagram of the surface roughness measured along a circle on the (111) plane is shown in Fig. 12.

Comparing experimental results of the anisotropic properties of machined surface roughness shown in Fig. 12 with the simulation results of dislocation emissions of the machined crystal plane, they can be seen to be essentially consistent.

The experimental results show that surface roughness in the [112] direction is slightly less than in the [112] direction. The reasons for this phenomenon can be explained from the simulation process. The main reason may be because of a phenomenon that occurs in simulation process, i.e., when cutting in the [112] direction, there are more dislocations emitted from the crystalline plane below the machined surface, and fewer dislocations emitted from the crystalline plane above the machined surface. Therefore, when damage occurs in single-crystal silicon, cracks at the top of the machined surface can be removed by subsequent turning.

However, though the number of dislocations emitted in the [112] cutting direction is the same as in the [112] cutting direction, the dislocations are distributed in an opposite fashion. Thus, when plastic deformation under the machined surface does not easily form, then fracture failure is liable to occur, and the cracks are also more easily extended to the machined surface under the action of the cutting tool, resulting in the deterioration of surface quality.

The AFM images of the surface topography of the (100) plane in cutting directions 0°, 15°, 30°, and 45° are shown in Fig. 13. A schematic diagram of continuous measurement of the roughness along a circle on the (100) plane is displayed in Fig. 14. A group of smaller cutting parameters with a_p=3 μm and f=0.8 μm/rev was used to perform the turning experiment, as the silicon (100) plane does not easily form a mirror machined surface. Comparing experimental results with simulation results of dislocation emissions of the machined (100) crystal plane, they are also seen to be essentially consistent.

4 Conclusions

In this paper, simulation studies were performed on the mechanism of surface anisotropy, and in particular both the crystal structure and mechanical properties of single-crystal silicon were simultaneously taken into account for the first time. The following conclusions can be drawn:

The anisotropic surface quality during ultra-precision turning of single-crystal silicon is caused by the number of dislocations in different directions along the cutting plane and also by the uneven distribution of the dislocations between the machined plane and the slip planes under the action of the cutting tool. Moreover, the turned surface has six higher quality parts and six lower quality parts in the form of a sixfold symmetric cross through the center when turning on the (111) crystal plane. In addition, the turned surface has four higher quality parts and four lower quality parts in the form of a fourfold symmetric cross through the center when turning on the (100) and (110) crystal planes.

The surface quality of single-crystal silicon is determined jointly by the number of dislocations on the machined surface and on the crystal surface, namely, the greater the number of dislocations on the machined surface and the more even the distributed dislocations between the machined surface and the slip planes, the better the surface quality. Therefore, machined surface quality is best when machining along the (111) crystal plane. The simulation results also showed that the use of a −40° rake angle tool can achieve better surface quality.

References

1. Leung TP, Lee WB, Lu XM (1998) Diamond turning of silicon substrates in ductile regime. J Mater Process Technol 73:42–48
2. Jasinevicius RG, Pizani PS (2007) Annealing treatment of amorphous silicon generated by single point diamond turning. Int J Adv Manuf Technol 34:680–688
3. Yan J, Syoji K, Kuriyagawa T, Suzuki H (2002) Ductile regime turning at large tool feed. J Mater Process Technol 121:363–372
4. Fang FZ (1998) Nano-turning of single crystal silicon. J Mater Process Technol 82:95–101
5. Yan J, Syoji K, Kuriyagawa T (2002) Fabrication of large-diameter single-crystal silicon aspheric lens by straight-line enveloping diamond-turning method. J Jpn Soc Precis Eng 68 (4):1561–1565
6. Sharif UM, Seah KHW, Rahman M, Li XP, Liu K (2007) Performance of single crystal diamond tools in ductile mode cutting of silicon. J Mater Process Technol 185:24–30
7. Blackley WS, Scattergood RO (1991) Ductile regime model for diamond turning of brittle materials. Precis Eng 13:95–102
8. Fang FZ, Wu H, Liu YC (2005) Modeling and investigation on machining mechanism of nano-cutting monocrystalline silicon. Int J Mach Tools Manuf 45:1681–1686
9. Inamura T, Shimada S, Takezawa N, Nakahara N (1997) Brittle/ductile transition phenomena observed in computer simulations of machining defect-free monocrystalline silicon. Ann CIRP 46:31–34
10. Yan J (2004) Laser micro-Raman spectroscopy of single-point diamond machined silicon substrates. J Appl Phys 95:2094–2101
11. Tanikella BV, Somasekhar AH, Sowers AT, Nemanich RJ, Scattergood RO (1996) Phase transformations during microcutting tests on silicon. Appl Phys Lett 69:2870–2872
12. Morris JC, Callahan DL, Kulik J, Patten JA, Scattergood RO (1995) Origins of the ductile regime in single-point diamond turning of semiconductors. J Am Ceram Soc 78:2015–2020
13. Fang FZ, Wu H, Zhou W, Hu XT (2007) A study on mechanism of nano-cutting single crystal silicon. J Mater Process Technol 184:407–410
14. Blake PN, Bifano T, Scattergood RO (1988) Precision machining of ceramic materials. Ceram Bull 67:1038–1044
15. Blake PN, Scattergood RO (1990) Ductile-regime machining of germanium and silicon. J Am Ceram Soc 73:946–957
16. Blackley W, Scattergood RO (1990) Crystal orientation dependence of machining damage—a stress model. J Am Ceram Soc 73 (10):3113–3115
17. Shibata T, Fujii S, Makino E (1996) Ductile-regime turning mechanism of single-crystal silicon. Precis Eng 18:129–137
18. Gatzen HH, Beck M (2003) Investigations on the friction force anisotropy of the silicon lattice. Wear 254:1122–1126

19. Komandurib R, Chandrasekaran N, Raff LM (1999) Orientation effects in nanometric cutting of single crystal materials: an MD simulation approach. Ann CIRP 48(1):67–72
20. Hung NP, Fu YQ (2000) Effect of crystalline orientation in the ductile-regime machining of silicon. Int J Adv Manuf Technol 16:871–876
21. Cheung CF (2003) Influence of cutting friction on anisotropy of surface properties in ultra-precision machining of brittle single crystals. Scripta Mater 48:1213–1218
22. Connor BPO, Marsh ER, Couey JA (2005) On the effect of crystallographic orientation on ductile material removal in silicon. Precis Eng 29:124–132
23. Marsh ER, Sommer EJ, Deakyne TRS, Kim GA, Simonson JA (2010) Detection of orientation-dependent, single-crystal diamond tool edge wear using cutting force sensors, while spin-turning silicon. Precis Eng 34:253–258
24. Wang MH, Lu ZS (2007) The theoretical study on the mechanism of BDT in machined Si single crystal. Key Eng Mater 339:84–89
25. Wang MH, Lu ZS (2008) Study on brittle-ductile transition of ultra-precision turning of single crystal silicon. Key Eng Mater 375–376:11–16
26. Evans AG, Marshall DB (1980) Wear mechanisms in ceramics. In: Rigney DA (ed) Fundamentals of friction and wear of materials. American Society for Metals, Metals Park, pp 439–452
27. Zhang Q, Cai CR, Zhou HF (2001) TEM observations of the dislocations from micro-indentation surface in single crystalline silicon at room temperature. J Fuzhou Univ (Natural Science) 29 (2):55–58
28. Rice JR (1992) Dislocation nucleation from a crack tip: an analysis based on the peierls concept. J Mech Phys Solids 40 (2):239–271
29. Williams ML (1957) On the stress distribution at the base of stationary crack. J Mech Phys Solids 24:109–114
30. Rice J, Thomson RR (1974) Ductile versus brittle behavior of crystals. Philos Mag 29(1):73–97
31. Wang TC (1998) Dislocation theory of the fracture criterion for anisotropic solids. Philos Mag 77(1):31–53
32. Thomson R (1978) Brittle fracture in a ductile material with application to hydrogen embrittlement. J Mater Sci 13(1):128–142
33. Sih GC (1974) Strain-energy-density-factor applied to mixed mode crack problems. Int J Fract 10(3):305–321